(NASA-CR-163950) TURBINE ENDWALL TWO-CYLINDER PROGRAM Semiannual Status Report, 1 Jul. 1980 - 1 Jan. 1981 (Connecticut Univ.) 38 p HC A03/MF A01 CSCL 20D G3/34

N81-17384

Unclas 41441

MECHANICAL ENGINEERING DEPARTMENT

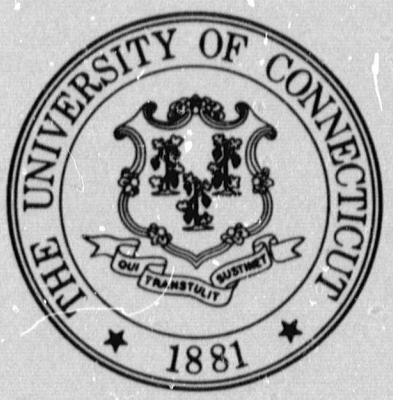

SCHOOL OF ENGINEERING
THE UNIVERSITY OF CONNECTICUT

STORRS, CONNECTICUT

TURBINE ENDWALL TWO-CYLINDER PROGRAM

Semi-Annual Status Report

Grant No. NSG 3238

July 1, 1980 - January 1, 1981

Submitted to:

Lewis Research Center
National Aeronautics and Space Administration
21000 Brookpark Road
Cleveland, Ohio 44135

Principal Investigator:

Lee S. Langston
Associate Professor
Department of Mechanical Engineering
University of Connecticut
Storrs, Connecticut 06268

Introduction

The following is a report of progress made during the fourth six-month period (July 1, 1980 to January 1, 1981) under NASA Grant No. NSG 3238, "Turbine Endwall Two Cylinder Program". Under this grant an analysis and a series of experiments are being carried out to study the three-dimensional separation of fluid flow around two isolated cylinders mounted on an endwall.

The work reported comes under Tasks I and II of the program and deals with:

a) water tunnel testing for both the single and double cylinder cases.

b) wind tunnel flow characteristics.

c) static pressure distribution measured on the cylinders.

d) design and construction of a pressure reference system.

e) overview.

Water Tunnel Testing

Boundary layer flow past a single cylinder mounted on an endwall has been investigated by a number of researchers (Ram[1], Peake and Galway[2], East and Hoxey[3], Belik[4], Baker[5,6] and others). Ram[1] presented data for a single horseshoe vortex flow at the endwall cylinder junction. Baker[5,6] found that under certain conditions multiple as well as oscillating vortices can occur. Herein, we have presented saddle point location data, for both the single and double cylinder cases, taken at low velocity in the water tunnel.

The turbulence manipulators used at the water tunnel test section inlet have been discussed in a previous progress report[7]. Although these manipulators have straightened out the flow so that it is adequate for data acquisition, a small amount of bulging in the velocity profiles near the endwalls was

observed. Laws and Livesey[8] suggest that this happens when k values are greater than 1. Schubauer, Spangenburg and Klebanoff[9] found a k value of 2.8 to be the optimum for making an arbitrary flow uniform. Our k is much larger than this.

As was mentioned in the last progress report[10], boundary layer velocity measurement is complicated by the fact that our hot-wire probe is not temperature compensated and therefore drifts slowly as the water temperature changes. Another difficulty encountered while making this velocity measurement is that caused by air coming out of solution and forming bubbles in the water. These air bubbles often adhere to the hot-wire and change the local heat transfer coefficient. The difficulties we have had measuring a velocity profile are important because without the profile we cannot calculate either a shape factor or a displacement thickness. Without a good shape factor measurement, we have not been able to determine the boundary layer type (laminar or turbulent); however, we have used the voltage output of the hot-wire anemometer system to obtain an approximate boundary layer thickness and to observe that the shape factor varies significantly with main stream velocity.

The method used for visualizing and locating saddle points was described in the last progress report[10]. Some sample limiting streamline photographs, for various cylinder diameters, are shown in figure 1. These photographs are taken from above the test section and they show the limiting streamline pattern on the floor. The saddle points are identified by small dots.

Both Belik[4] and Baker[5,6] have done dimensional analyses for the single cylinder problem. In Baker[5] it is assumed that saddle-point standoff distance depends on the following parameters:

$$R = fn(D,\ell,U,\delta^*,H,u',\mu,\rho) .$$

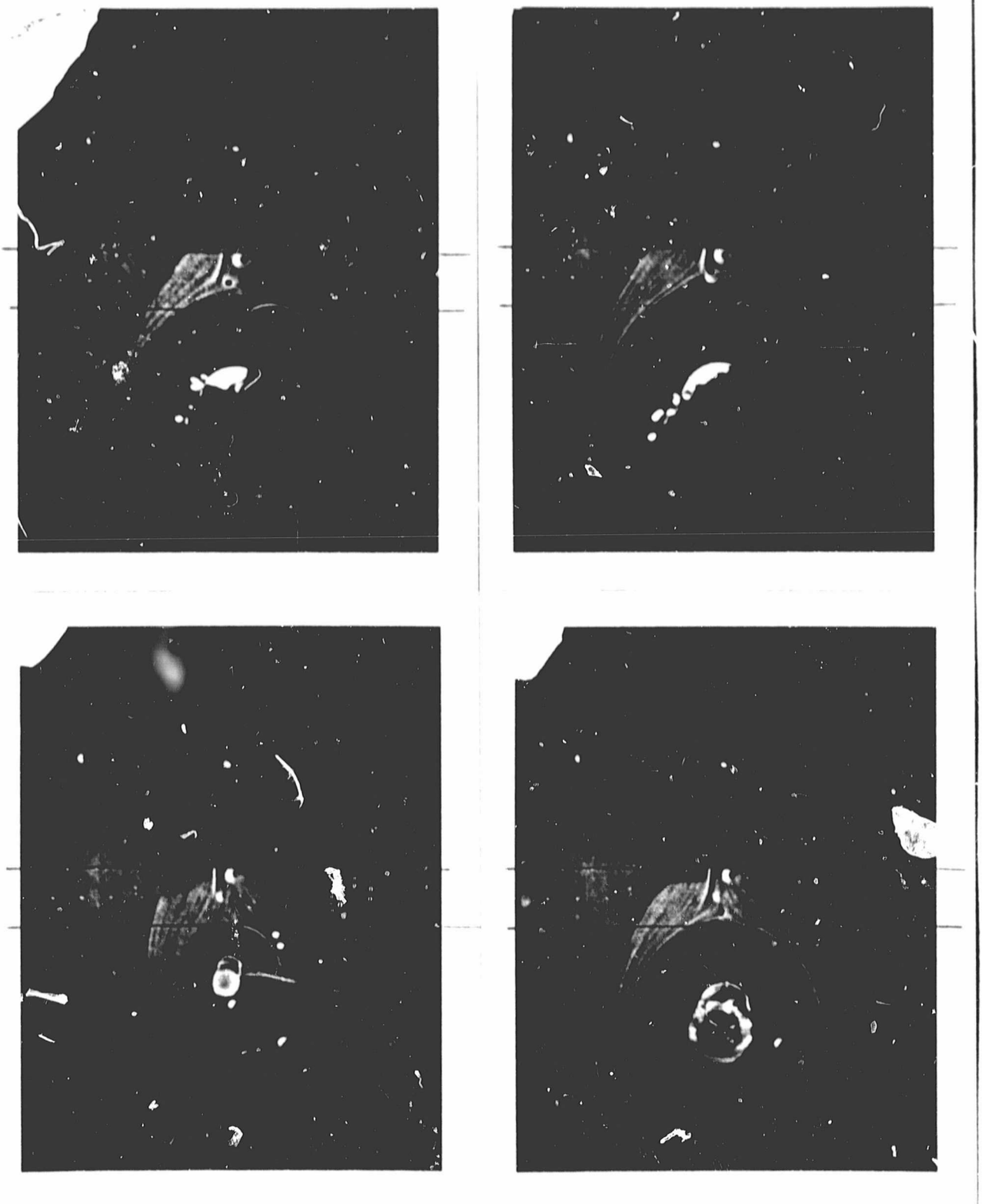

Figure 1 - Sample limiting streamline phototograph

Non-dimensionalizing gives

$$R/D = fn\left(\frac{UD}{\nu}, \frac{D}{\ell}, \frac{D}{\delta^*}, H, \frac{u'}{U}\right). \qquad (1)$$

For the cases presented in this report, D/ℓ is small and it is assumed that the value of R/D does not depend on this dimensionless group. The variations in turbulence distribution throughout the boundary layer have not been considered. For the presentation of our water tunnel data we have not considered variations in H to be as important as UD/ν or D/δ^*. This removal of H from our list of independent variables is shown to be valid (for our limited test conditions) by the data presentation. In this report we have used boundary layer thickness rather than displacement thickness as a variable. So then, we are left with the following dimensionless groups:

$$R/D = fn\left(\frac{UD}{\nu}, \frac{\delta}{D}\right). \qquad (2)$$

Figures 2 and 3 show the coordinate systems used to locate the saddle points for the single and double cylinder cases respectively.

We have taken the single cylinder saddle point location data for the following reasons:

1. To visualize and become familiar with the flow before embarking onto the two cylinder case.
2. To establish a data acquisition routine using a less complicated flow than the two cylinder case.
3. To compare our results with that of other investigators.

Figure 4 is a plot of non-dimensional saddle point location, (R/D), versus Reynolds number based on cylinder diameter, taken in our water tunnel, for the single cylinder case, for three different free stream velocities and

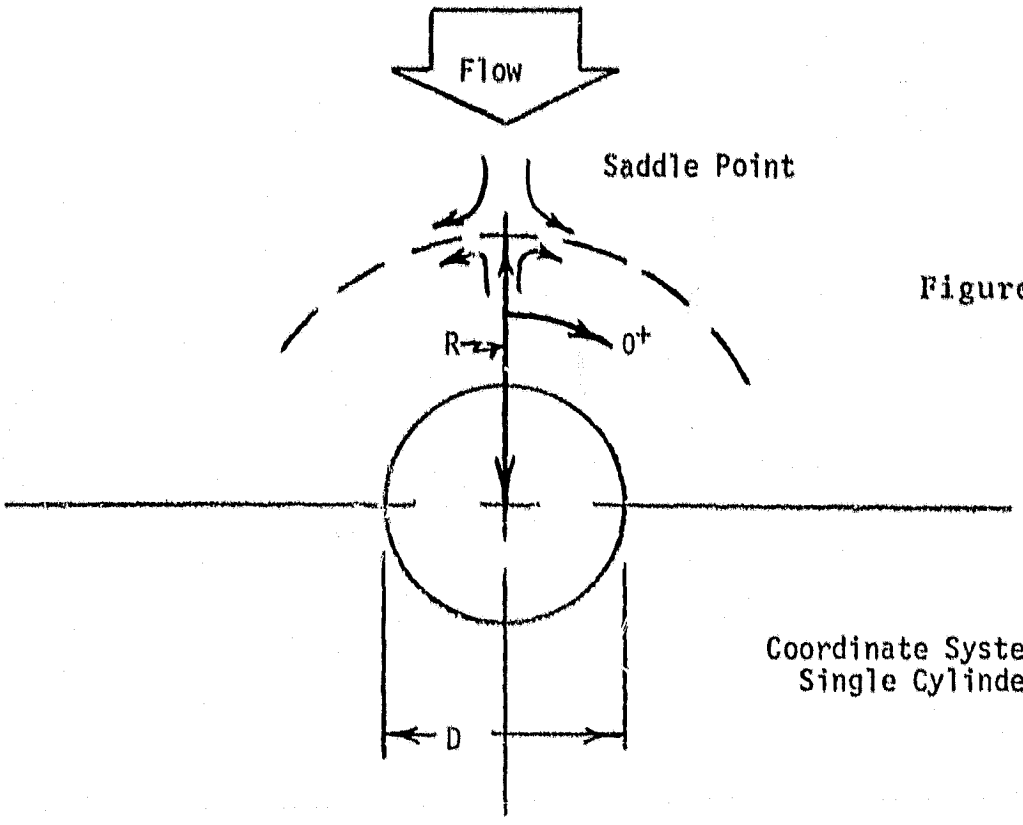

Figure 2

Coordinate System For
Single Cylinder

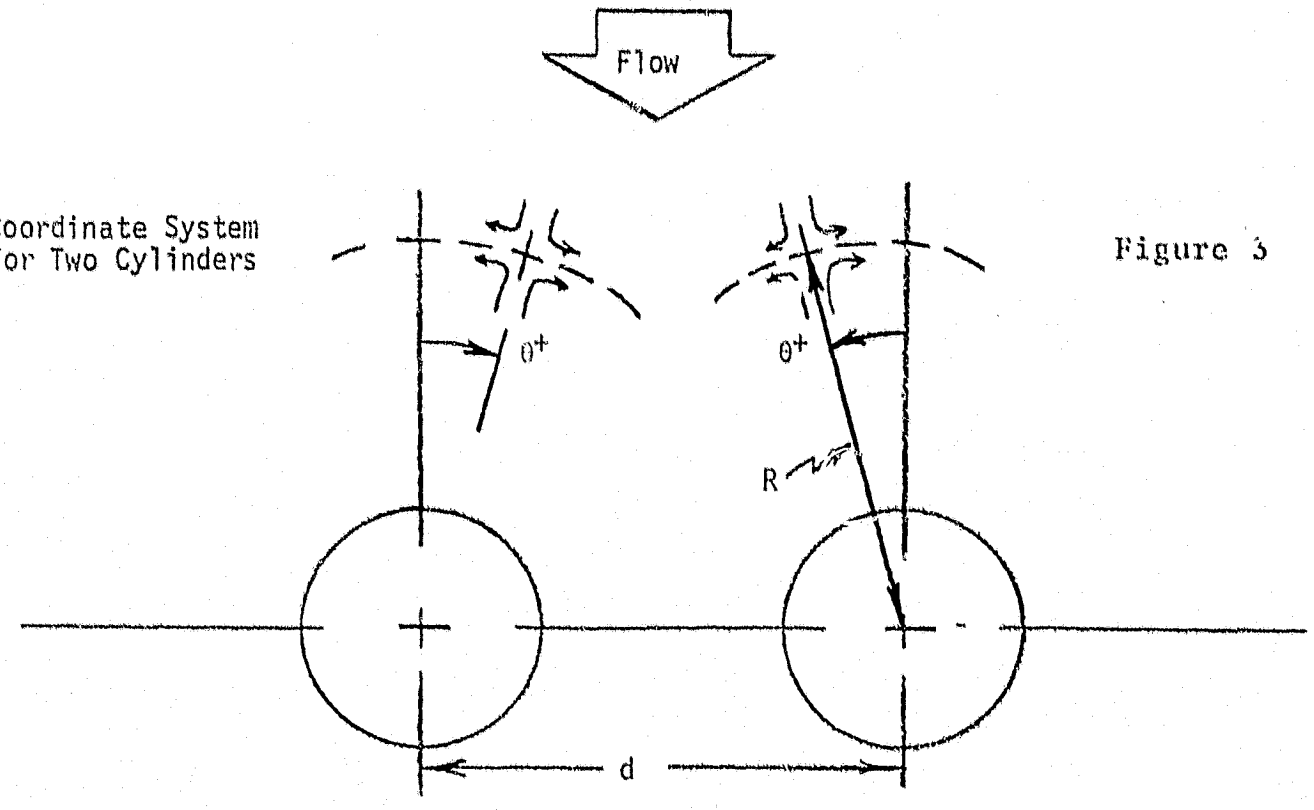

Coordinate System
For Two Cylinders

Figure 3

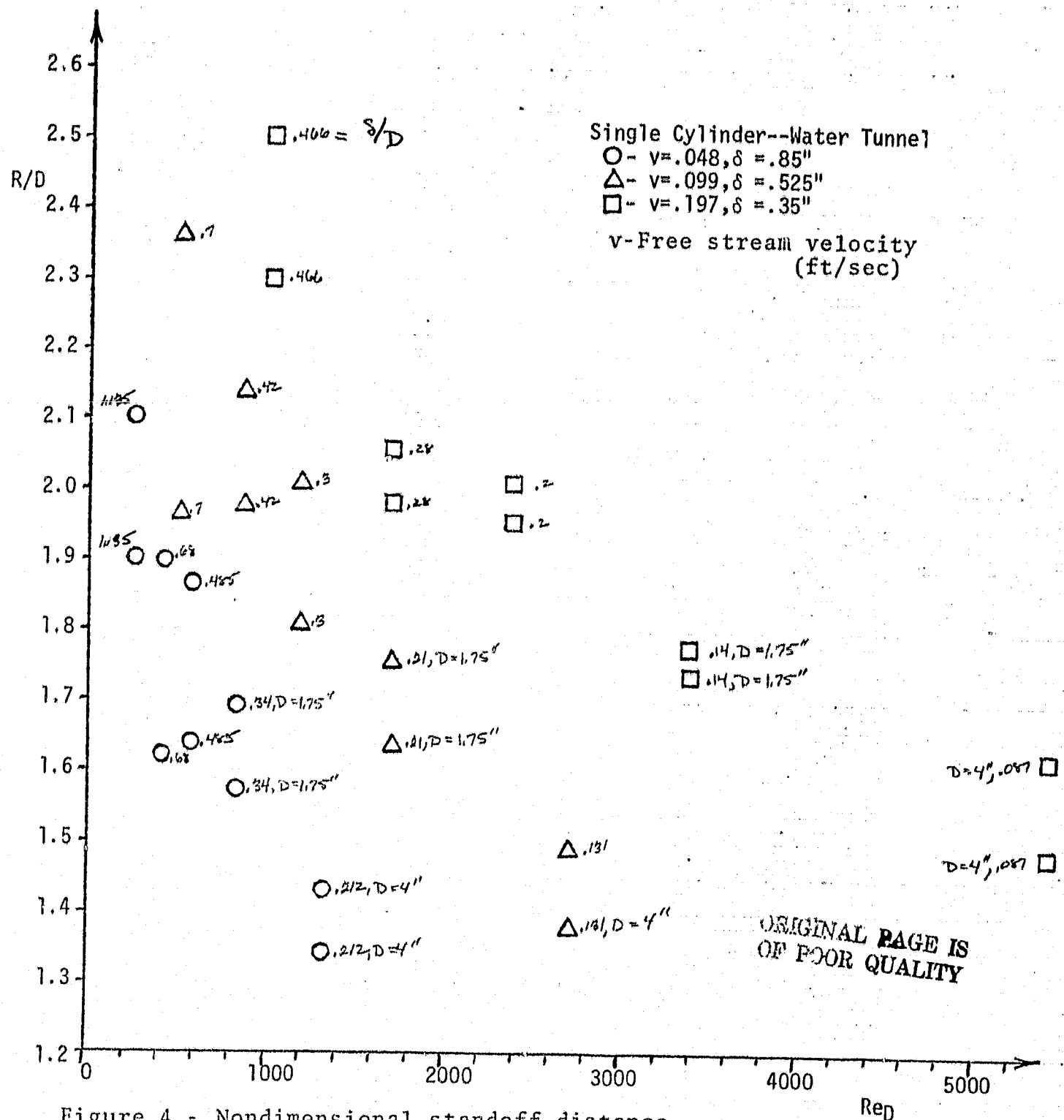

Figure 4 - Nondimensional standoff distance vs Reynolds number

five different cylinder diameters at each of those velocities. The values of δ/D are recorded along the side of each data point and two of the cylinder diameters are indicated in the same fashion. Figure 5 is a plot of the same data using R/D and δ/D as coordinate axes and the values of Re_D are recorded. In figure 5 it can be seen that at a constant value of δ/D the magnitude of R/D increases quite strongly with increasing Re_D. Figure 4 shows that at a constant value of Re_D, R/D increases strongly with increasing δ/D. In both his paper [5] and thesis [6], Baker points out that increasing the flow velocity past a given cylinder does not affect saddle point location. It can, in fact, be seen in figure 4 that increasing Re_D by increasing U does not have a strong effect on R/D. The implication is that U is not an important variable. This is not at all the case as is evident by the trends of $R/D = fn(Re_D, \delta/D)$ just discussed. Increasing U and therefore Re_D holding all other variables constant tends to increase R/D; however, increasing U also decreases δ/D and therefore a tendency to decrease R/D is simultaneously enacted. The combination of these two effects yields a weak increasing function of R/D with increasing U.

Figure 6 is a plot of the water tunnel data given in figures 4 and 5 using the coordinates R/δ vs. Re_D. These two coordinates include all of the independent variables, and the plot reveals a unique relationship between R/δ and Re_D. The functional relationship given by the non-dimensional analysis consists of three non-dimensional parameters, yet figure 6 shows that only two parameters are necessary to determine the saddle point location. The three variables that we have been dealing with are given in equation (2). Again, their relationship is given by:

$$R/D = fn(Re_D, \delta/D)$$

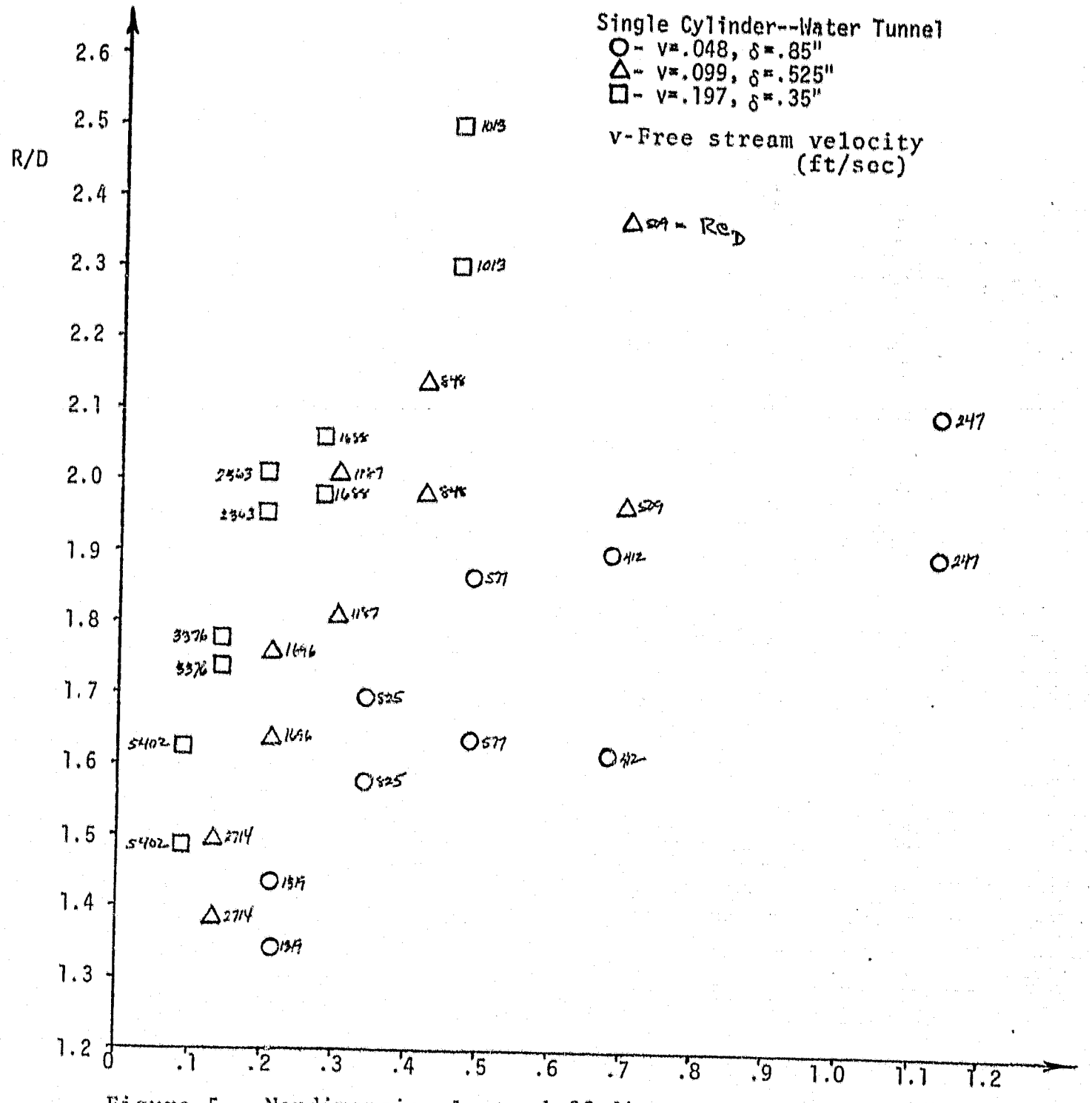

Figure 5 - Nondimensional standoff distance vs δ/D

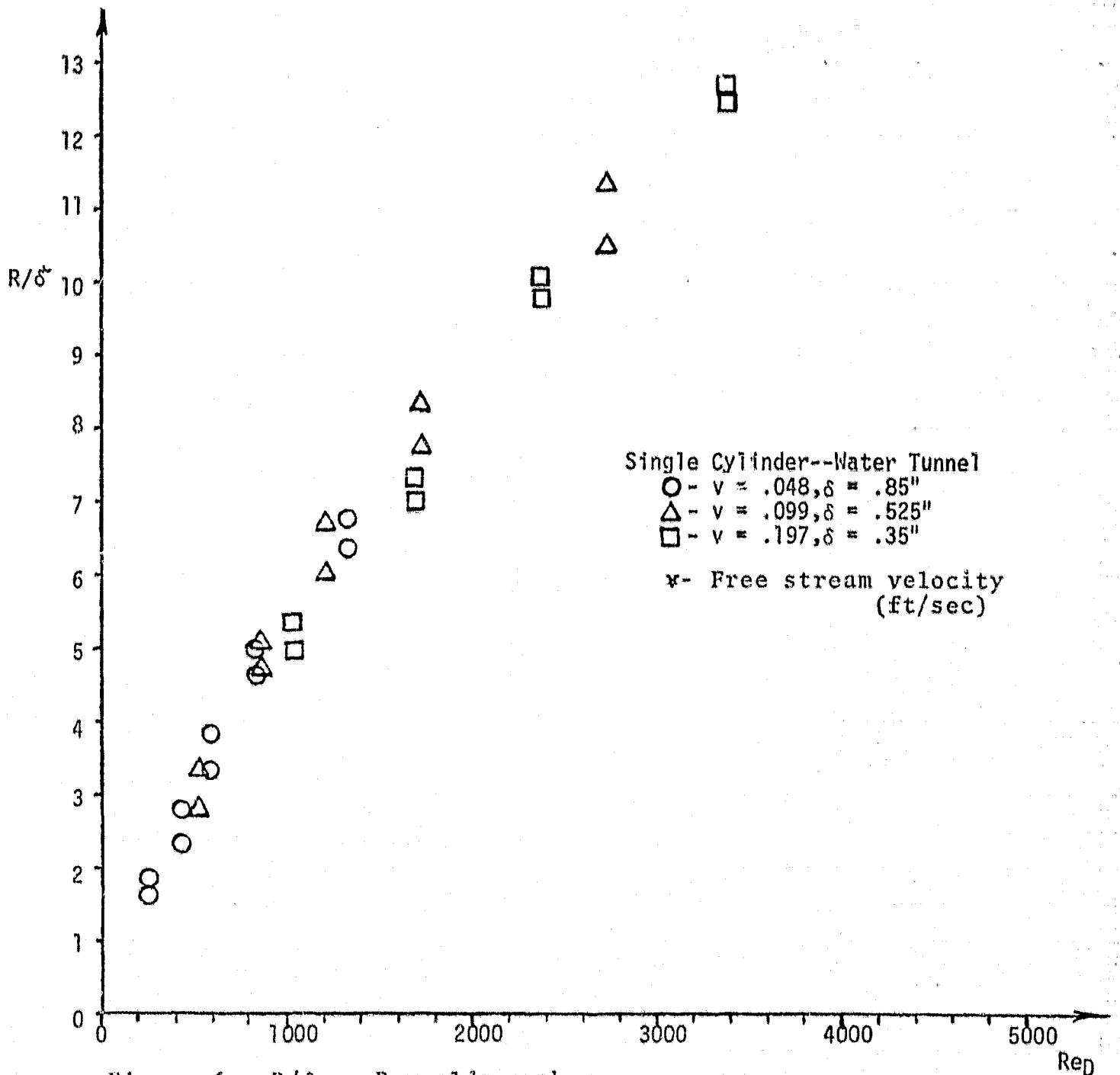

Figure 6 - R/δ vs Reynolds number

we have

$$R/\delta = \frac{R/D}{\delta/D} = \frac{D}{\delta} fn(Re_D, \delta/D) \tag{3}$$

and figure 6 shows that R/δ and Re_D are uniquely related so that

$$R/\delta = fn(Re_D) \tag{4}$$

eliminating R/δ between equations (3) and (4),

$$fn(Re_D) = D/\delta\ fn(Re_D,\ \delta/D) \tag{5}$$

In order for this to be true, the right hand side must be a function of only Re_D. For that to be the case, we must either have δ/D constant or δ/D and Re_D must be uniquely related. δ/D is not constant throughout the data of figure 6 so that the latter must be true.

So then, for our water tunnel

$$Re_D = \frac{UD}{\nu} = fn(\delta/D) \tag{6}$$

This is true if δ and U are uniquely related and that is indeed the case for a boundary layer developing on a fixed length of flat plate.

We can conclude that whenever we have flow past a cylinder mounted on an endwall where the saddle point position can be determined using the non-dimensional variables given in equation (2), and we also have a unique relationship between boundary layer thickness and free-stream velocity, that we will have a unique relationship between R/δ and Re_D.

A comparison of our single cylinder data to that of other researchers is given in figure 7. The wind tunnel data shown here is at much higher Reynolds numbers than our water tunnel data.

The one water tunnel study shown (Peake and Galway[2]) is for the case of a laminar boundary layer approaching the cylinder while all of the wind tunnel studies are for turbulent boundary layers. Peake and Galway's[2] data is for a fixed flow and four different cylinder diameters. Their boundary layer thickness is calculated using laminar flow - zero pressure gradient conditions (Blasius) and a flat plate length equal to the leading edge length on the endwall. This laminar boundary layer data falls very near the range of our water tunnel data.

Ram's[1] wind tunnel data is for a single Reynolds number (fixed U and D) and two different turbulent boundary layer profiles. The thinner of these two boundary layers (H = 1.56) developed in a natural way over the side wall flow surface, whereas the thicker boundary layer (H = 1.35) was achieved by means of plates installed on the side wall leading edge. Figure 7 shows that R/D increases with increasing δ/D.

East and Hoxey[3] give us one data point taken in a wind tunnel, at very high Reynolds number, for a turbulent incoming boundary layer.

Belik's[4] turbulent wind tunnel data was taken over ranges of free stream velocity, cylinder diameter and boundary layer thickness; however, it is presented in such a way that it is hard to isolate the effects of each. His curve fit yields R/D increasing with increasing δ/D and increasing Re_D.

For the purposes of this report the most useful data shown is that given by Baker[6], for a turbulent boundary layer, because he presents enough data so that we can compare trends. In Baker's paper for a laminar incoming boundary layer[5] there is a presentation of vortex position data that was obtained empirically; however, the saddle point position discussion is short and analytical. Figures 8, 9, and 10 are plots of Baker's[6] turbulent case data in the same coordinate systems used to present our own water tunnel data. His data

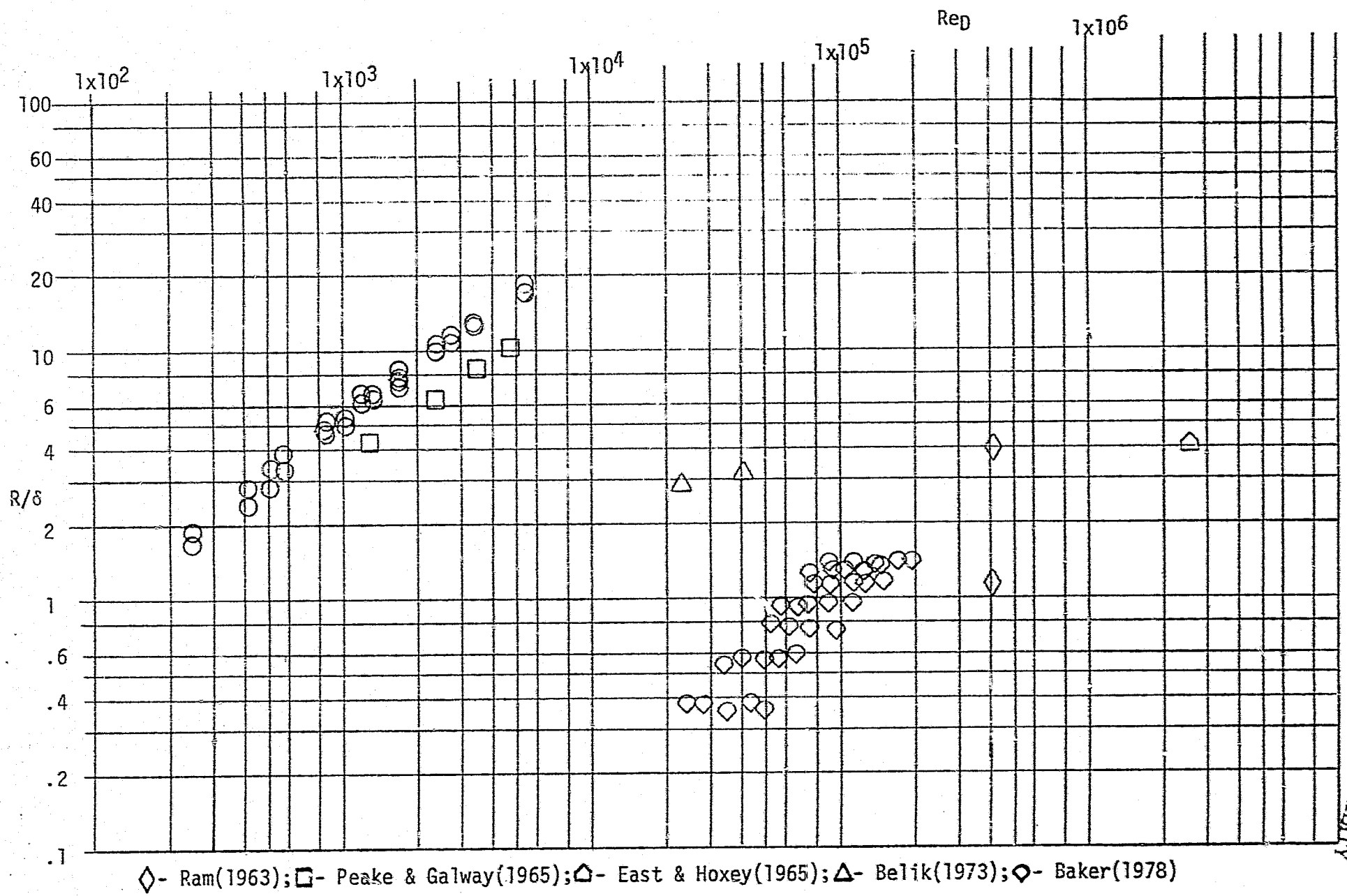

Figure 7 - Comparison of single cylinder standoff distance data - R/δ vs Reynolds number

is given in terms of δ^* so that in order to compare it to our data in terms of δ we have assumed a fully developed, flat plate, turbulent velocity profile ($H = 1.3$) where $\delta/\delta^* = 8.04$. There is quite a bit of scatter in the data; however, some overall trends can be observed. From figure 8 we can conclude that at constant Re_D, R/D increases as δ/D increases. This is consistent with our own water tunnel data; however, figure 9 shows that at constant δ/D, R/D decreases for increasing Re_D, opposite to that found in our water tunnel. When this turbulent (in air) data is plotted in the R/δ vs. Re_D coordinate system (figure 10) we do not have R/δ as a unique function of Re_D as we do for the data taken in our water tunnel. For Baker's[6] data we do have a unique relationship between δ and U as the data was taken in a fixed geometry test section. The implication here is that, over the range of flow conditions considered by Baker[6], there is some independent variable effecting saddle point position that is not considered in equation (2).

Our single cylinder study as well as the comparison of our data to the data of other investigators serves very well as a precursor to the double cylinder study. Although there is some disagreement between the trends found in our water tunnel experiment and Baker's[6] wind tunnel study we have identified the variables that are important to the prediction of saddle point location past an obstruction. Although the two cylinder case is an obstruction of different geometry than the single cylinder case we will show in the following section of this report that the coordinate system used to display the single cylinder data is a good base to start from in the description of the two cylinder data.

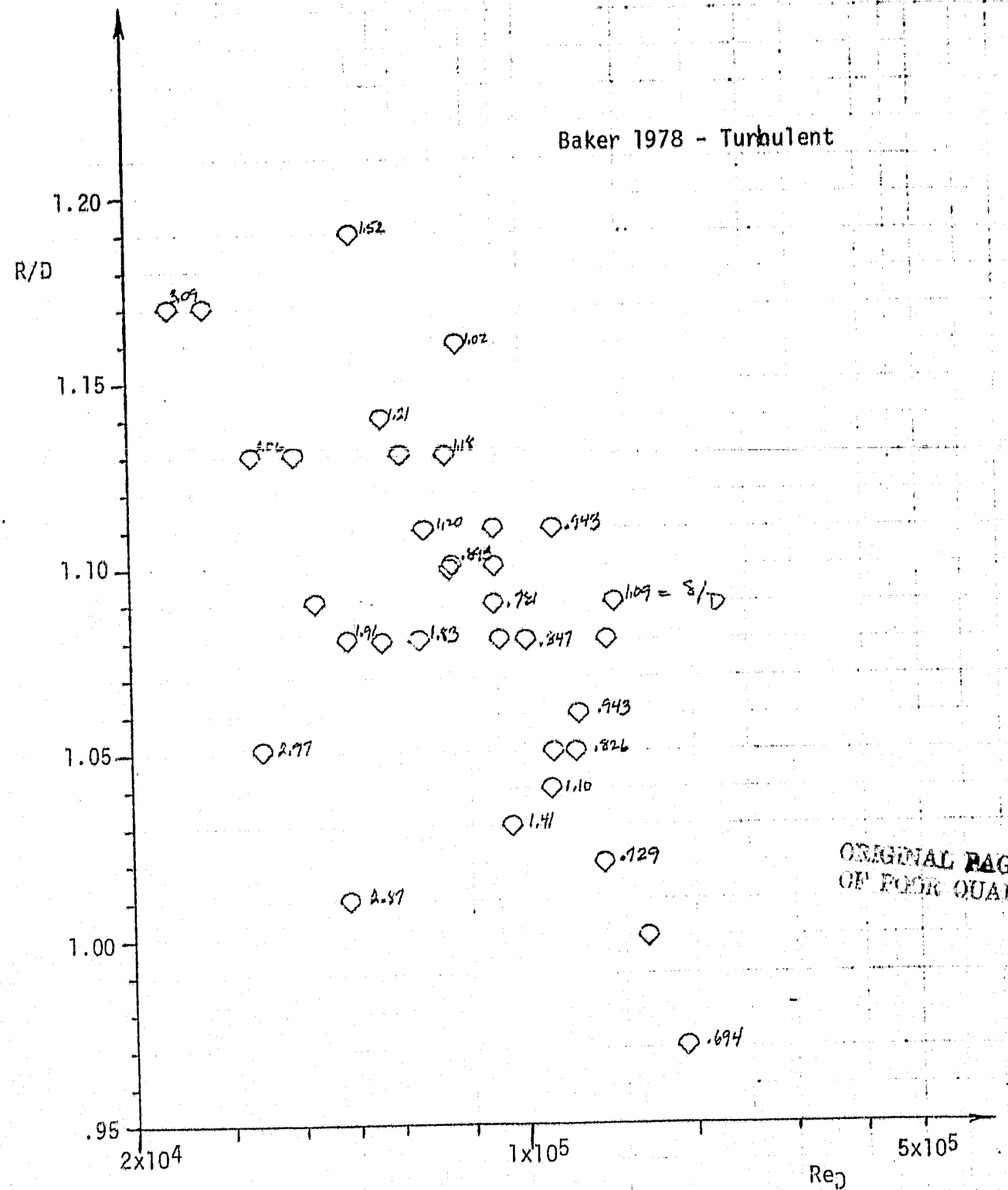

Figure 8 - Nondimensional standoff distance vs Reynolds number

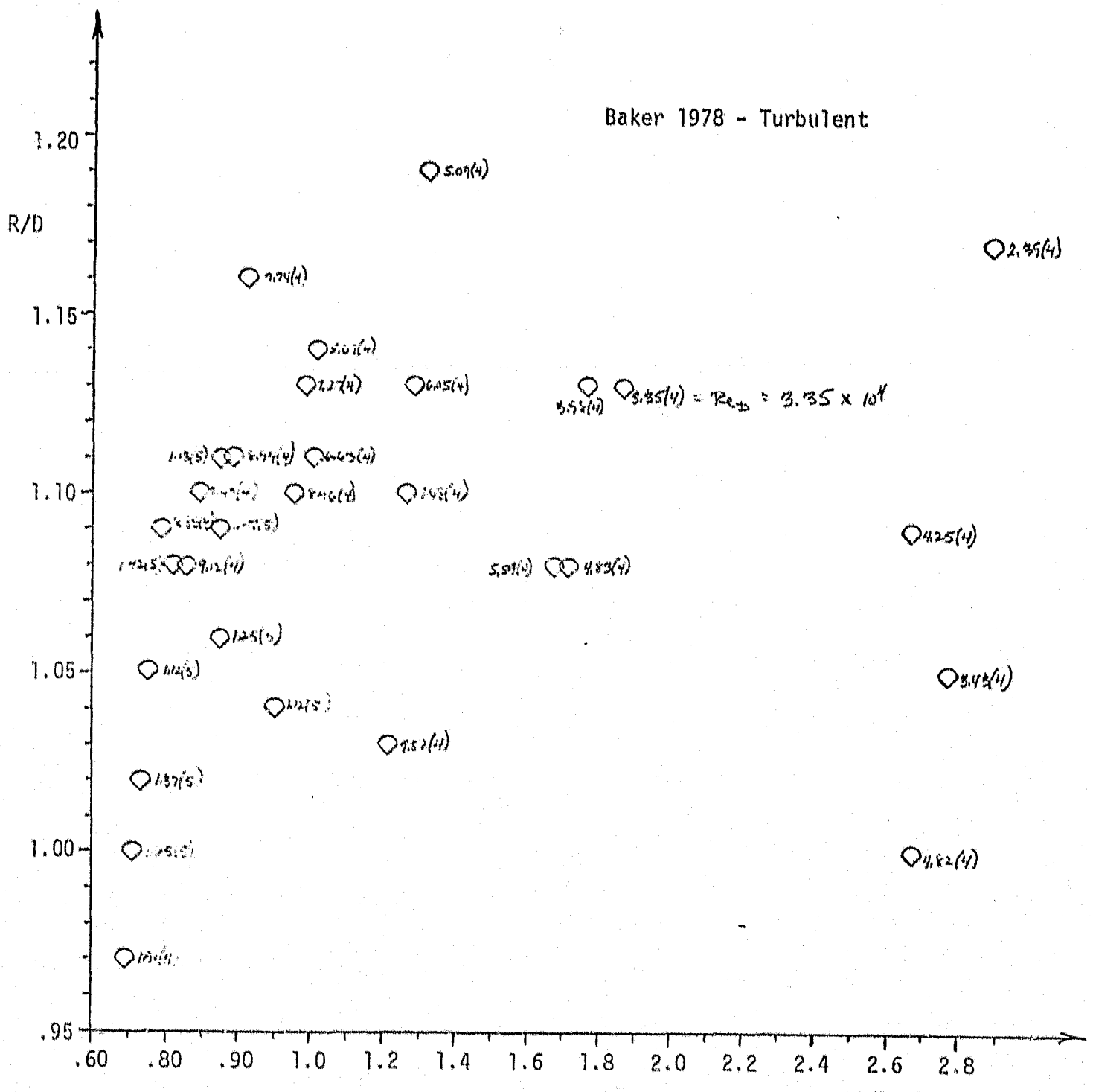

Figure 9 - Nondimensional standoff distance vs δ/D

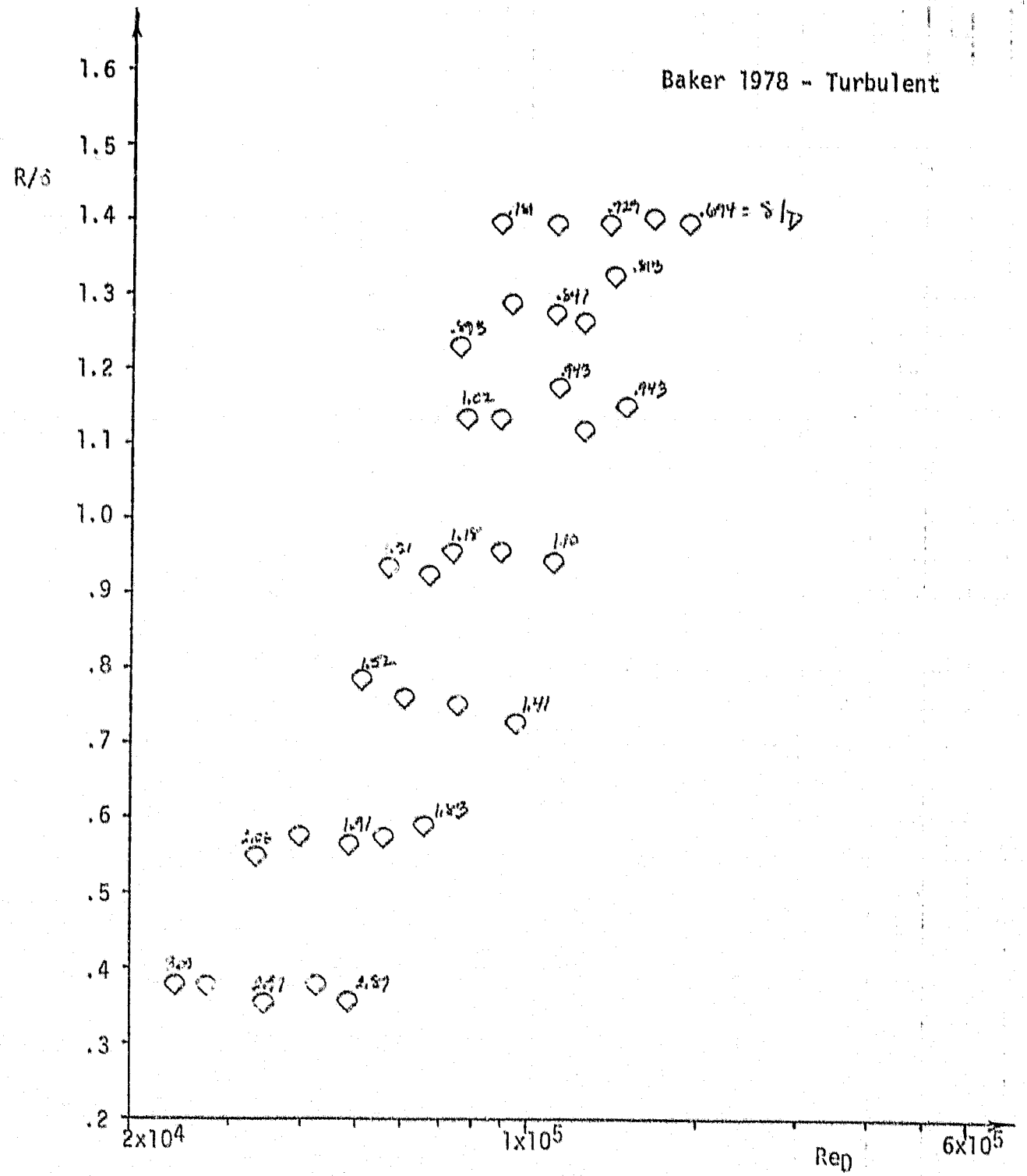

Figure 10 - R/δ vs Reynolds number

The data presented here is for flow past two cylinders mounted on an endwall in a low velocity flow of water. Referring to figure 3, we measure both saddle point standoff distance R and saddle point turning angle θ as a function of the following variables:

$$R = fn(V,D,\delta,d)$$

$$\theta = fn(V,D,\delta,d)$$

where d is the distance between the centers of the cylinders. Figure 11 is a plot of saddle point standoff distance versus non-dimensional cylinder separation, d/D, for one test section velocity and two cylinder diameters. Figure 12 is a plot of saddle point turning angle θ as a function of d/D for the D=1" case. At large cylinder separation there is a saddle point in front of each cylinder. As the two cylinders are brought closer together the saddle points start to turn in towards the other cylinder. The fact that the flow field around either cylinder is indeed being affected by the other cylinder is demonstrated by this turning.

The plot in figure 11 shows that the value of R is not strongly affected as d/D is decreased until a critical value of d/D is reached. At this critical cylinder separation, the two saddle points combine to form one saddle point, located on the centerline between the two cylinders and further upstream. Figure 11 shows that as d/D is decreased below this critical value, the standoff distance of this single saddle point increases markedly.

It is expected that at large cylinder separation the flow past either of the cylinders is as it would be for a single cylinder in the same flow. With this in mind we have plotted the data of figure 11 in the same coordinate system used for single cylinder data (R/δ vs. Re_D).

Figure 13 shows that prior to saddle point combination R/δ is a unique function of Re_D' as is the case for single cylinders. After saddle point

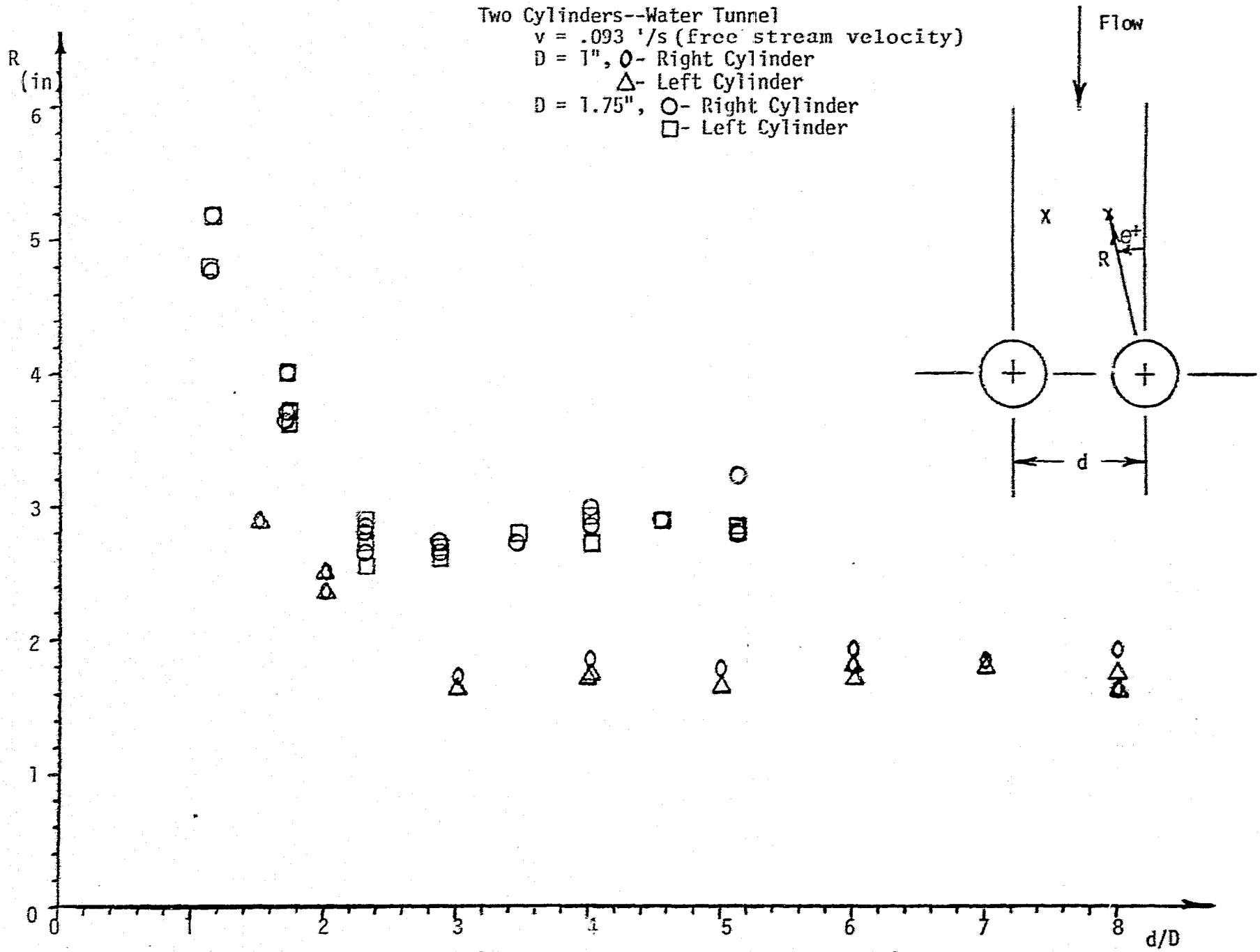

Figure 11 - Saddle point standoff distance vs cylinder separation

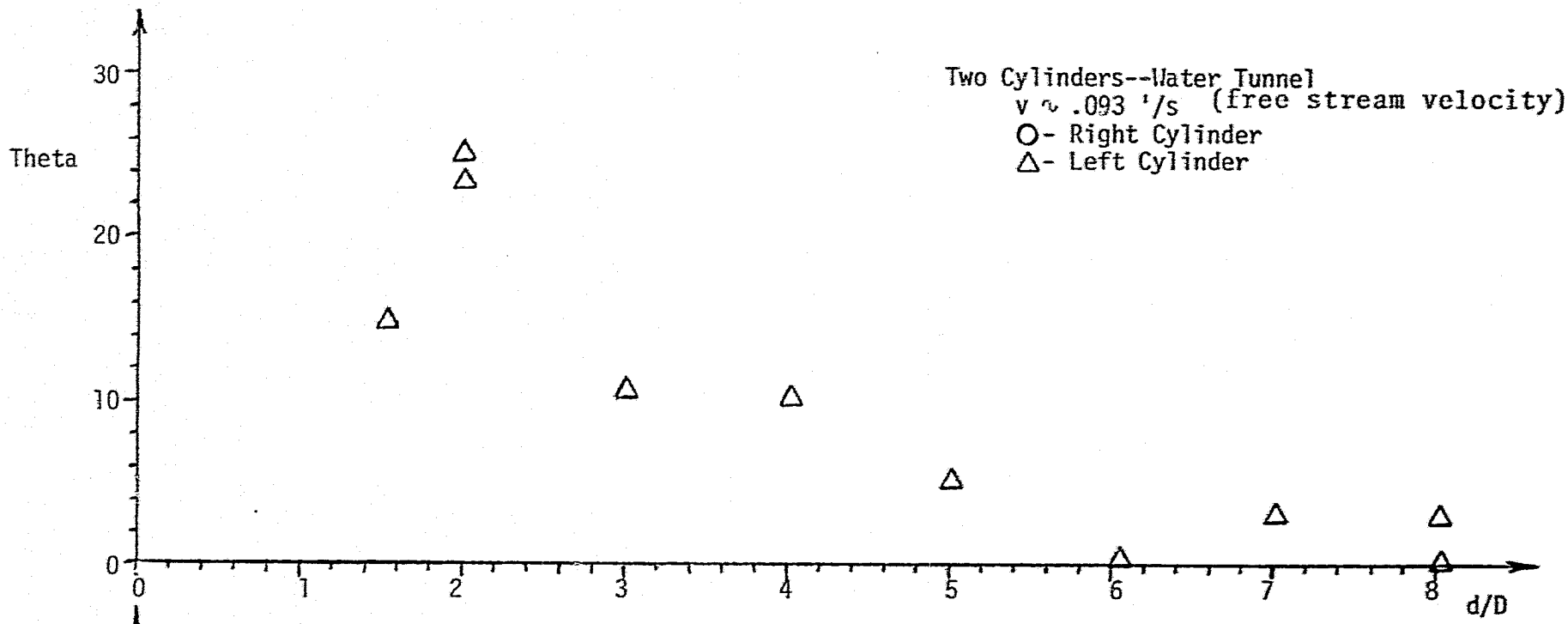

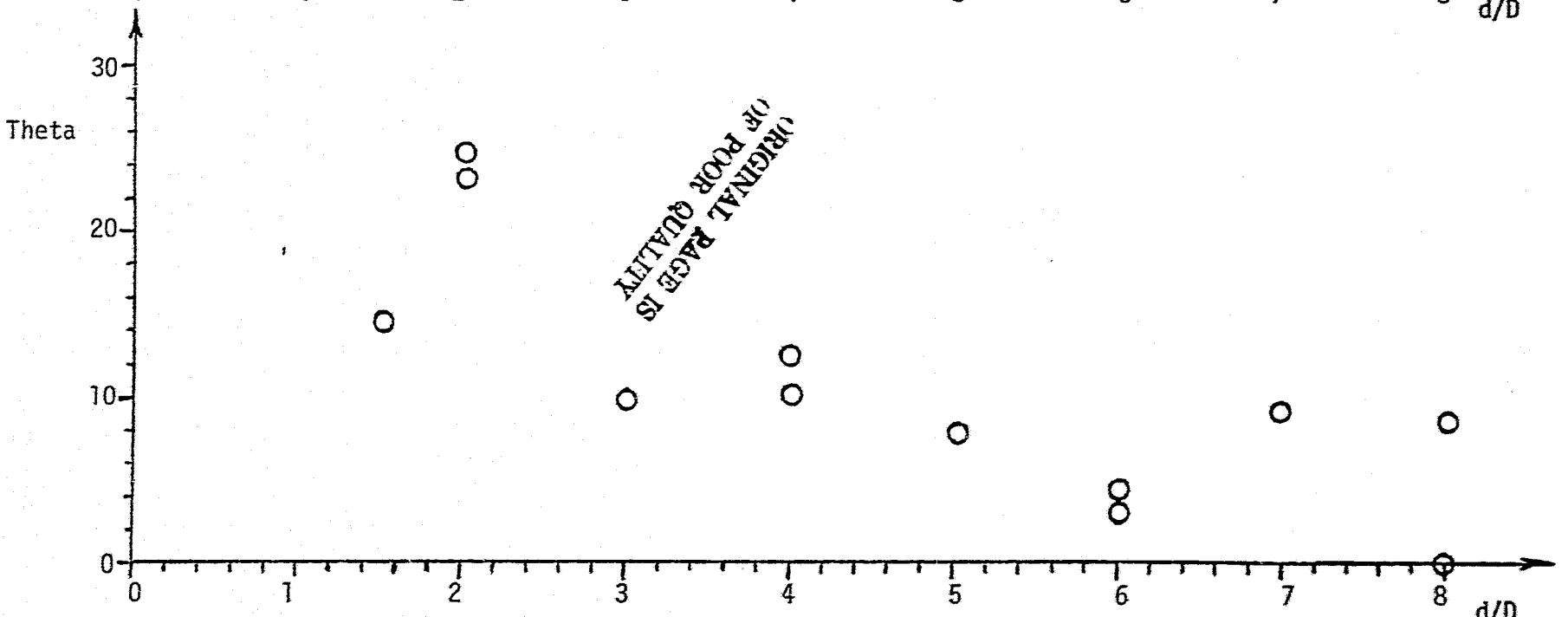

Figure 12 - Saddle point turning angle vs cylinder separation

combination this no longer holds true. The magnitude of the increase in R/δ upon combination is not a simple function of cylinder diameter and saddle point combination does not occur at a specific value of d/D.

Upon running the two cylinder experiment in the wind tunnel, we can expect that prior to saddle point combination the standoff distance will vary very much like it would for the same cylinder alone in the flow. However, after combination the two cylinders offer an obstruction whose geometry appears quite different to the flow than that prior to combination. In the wind tunnel, we have the free-stream velocity and the boundary layer thickness varying independently of one another so that even prior to combination we will not have a unique relationship between R/δ and Re_D.

Wind Tunnel Flow Characteristics

Our first evaluation of the test section flow characteristics revealed a boundary layer thickness that varied significantly as one traversed across either the upper or lower endwall (see figure 14) where the upper thickness was larger than the lower (figure 15). It was also found that both total pressure head and velocity head increased monotonically, by about 2.5 percent of main stream velocity head, as one traveled from north to south in the main stream flow (see figure 14). As reported in the last progress report[10], a total pressure mapping done at the inlet exit plane showed that both the boundary layer variations and the main stream non uniformity were present there as well. In an attempt to cause the transition from a laminar to a turbulent boundary layer to occur at the same streamwise location for all locations across the inlet a number of different boundary layer trip geometries were installed on the inlet floor (various streamwise locations along the contraction as well as multiple trips). The effects of the different trips

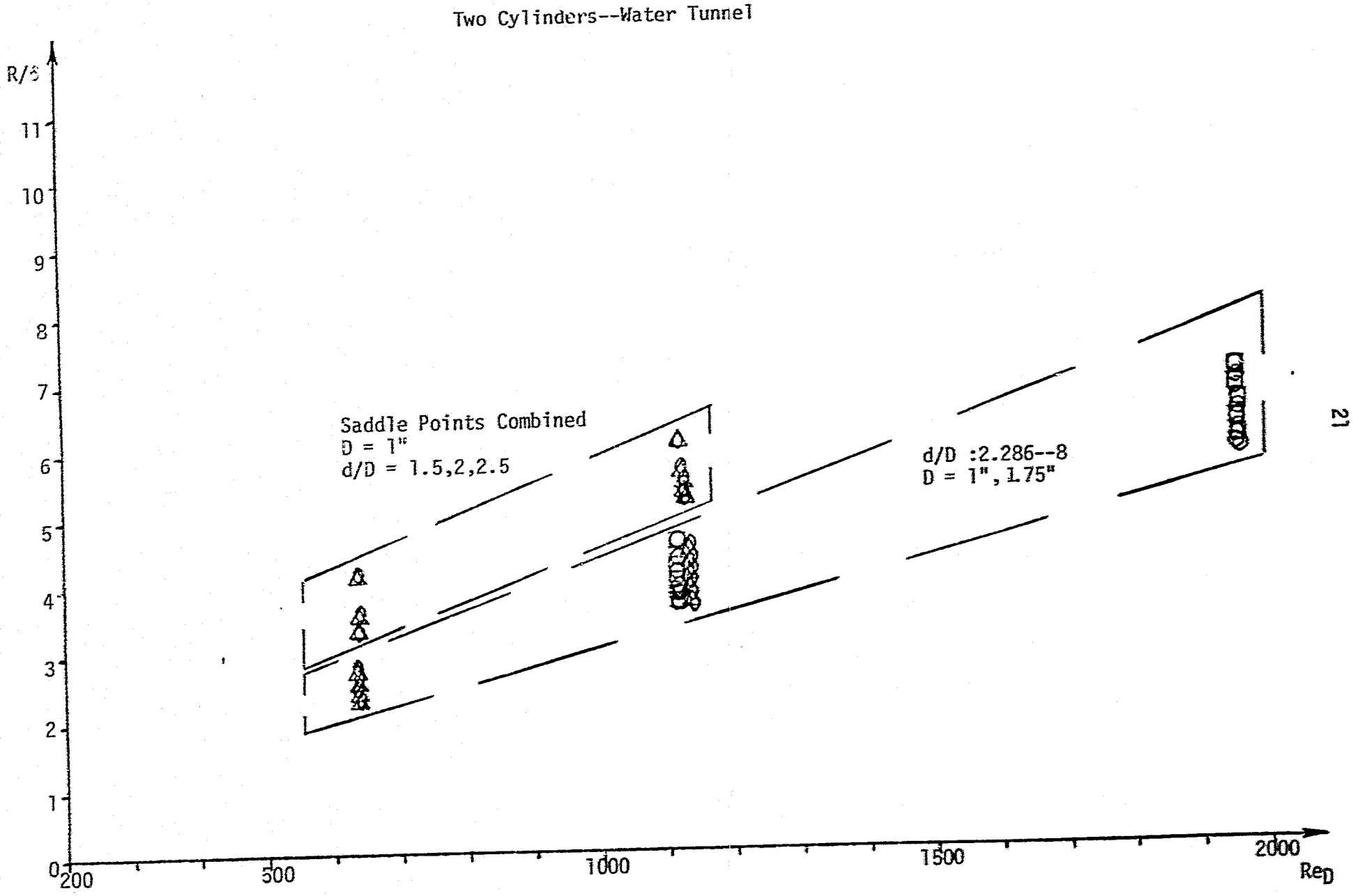

Figure 13 - R/δ vs Reynolds number

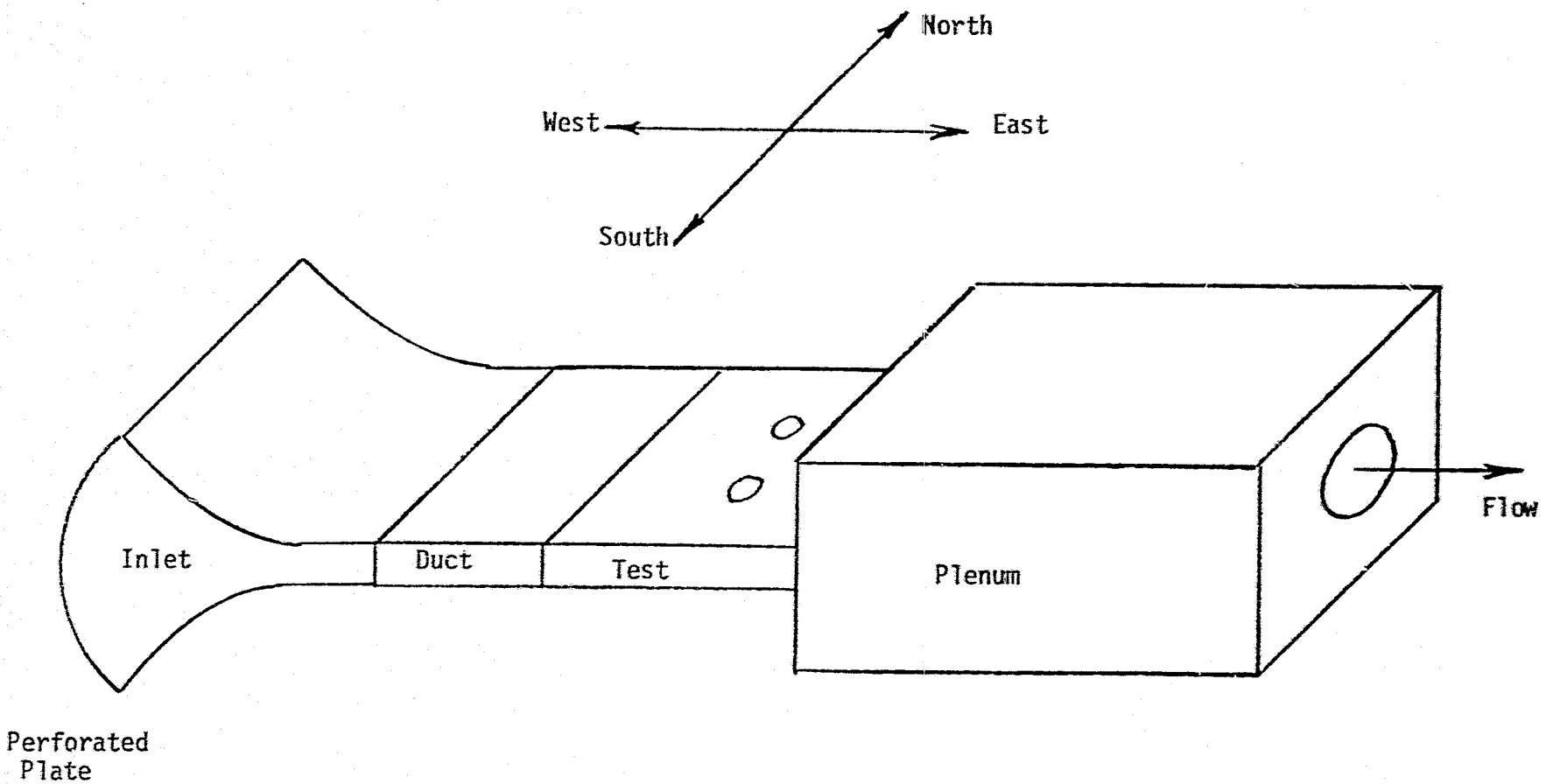

Figure 14 - Wind tunnel schematic

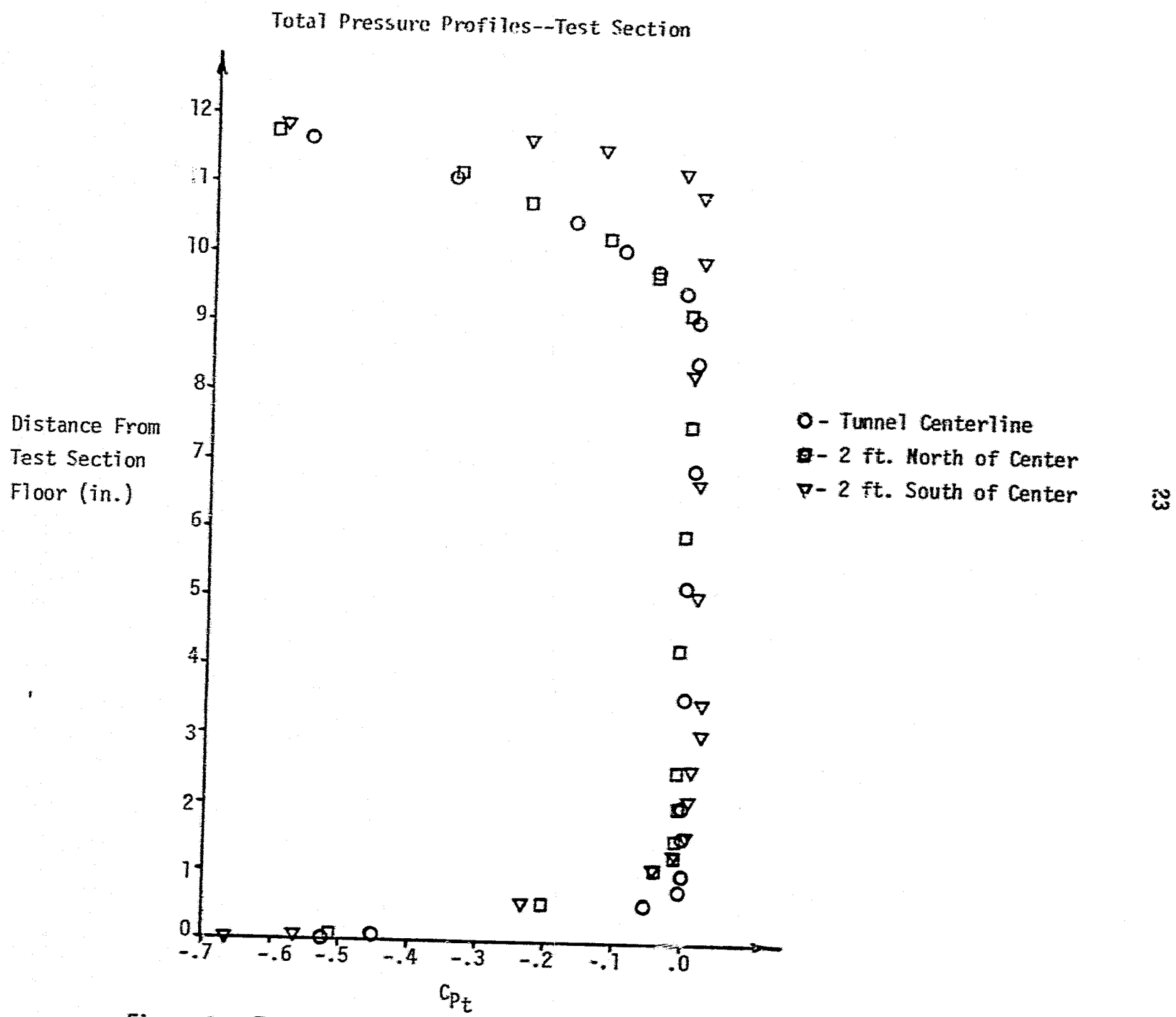

Figure 15 Total pressure profiles at the test section.

on the downstream flow were to increase the boundary layer thickness everywhere without eliminating the variations in thickness, implying that our problem was not one of transition. We then removed the honeycomb from the inlet entrance. A total pressure mapping shows that the boundary layer thickness has become much more uniform over the test section endwalls, particularly on the floor (figure 16) and that many of the main stream velocity profiles have become much more uniform. The reason for these changes could be that air had been leaking around the edges of the honeycomb causing variations in initial boundary layer thickness and that at some places the honeycomb was not knit tightly to the perforated plate, causing small nonhomogeneities in resistance over the cross section of the tunnel entrance (non uniform velocity profiles).

Although removing the honeycomb yielded significant improvements, we still had a small monotonic total pressure and velocity increase across the tunnel. Total pressure mappings both upstream and downstream of the perforated plate identified the perforated plate as the cause of this main-stream problem. Although the high resistance of the perforated plate makes the plate very effective for isolating the tunnel from the room (this has been verified by drastically altering the room flow with a large plywood baffle and observing that the tunnel flow was not changed), it is also the controlling factor for the flow downstream of it.

At present, with the honeycomb removed the maximum deviation in total pressure in the inviscid core of the test section is

$$\Delta C_{p_T} = \frac{\Delta(P_T - P_{T,\infty})}{(\frac{1}{2})\rho U_\infty^2} = 0.025 \qquad (3)$$

Static pressure was found to be constant across the test section. A simple

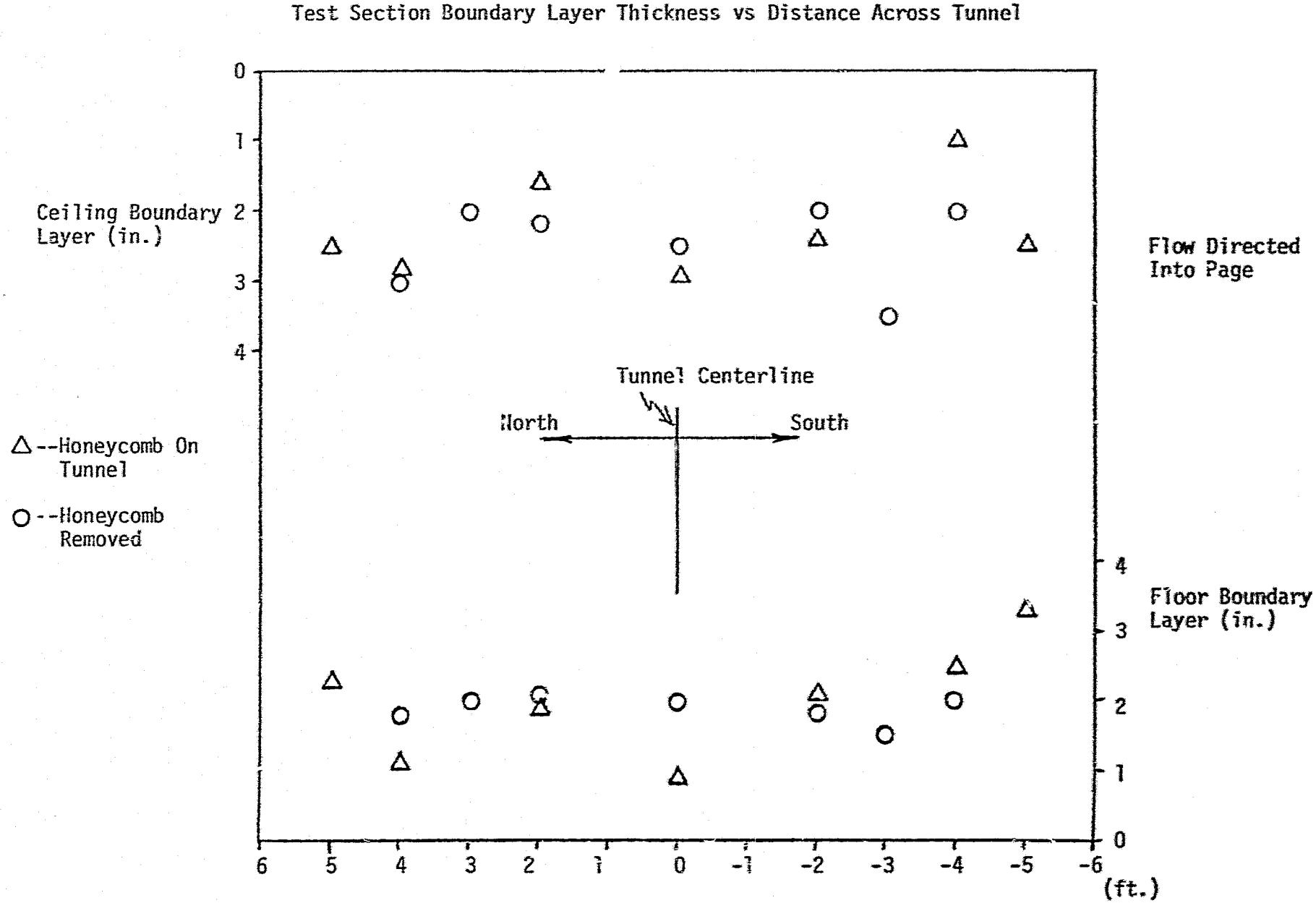
Test Section Boundary Layer Thickness vs Distance Across Tunnel
Ceiling Boundary Layer (in.)
0
1
2
3
4
Flow Directed Into Page
Tunnel Centerline
North
South
△--Honeycomb On Tunnel
○--Honeycomb Removed
Floor Boundary Layer (in.)
4
3
2
1
0
6
5
4
3
2
1
0
-1
-2
-3
-4
-5
-6
(ft.)

Figure 16

one-dimensional analysis shows that a variation in the hole diameters of the porous plate (nominal hole diameter of 0.0625 in. and porosity of 23%) of 0.0004 in could account for this small variation in total pressure. Such a variation could be caused by the paint on the plate itself.

Using the results of Schubauer, Spangenberg and Klebanoff[9], an additional porous plate of much higher porosity (40%) was installed at exit plane of the inlet. However, it was found that rather than making the flow in the test section more uniform, it distorted the flow.

This low resistance porous plate has been removed. At present we plan to add more resistance (screens on the porous plate of the inlet) on the side of the tunnel that has the highest total pressure. It should be emphasized that the variation given in equation (7) is small and correctable

As discussed in the last progress report[10], the mass of the centrifugal fan base was increased. The fan was then lifted off the floor and mounted on vibration dampers. A new flexible connection was installed between the fan and the diffuser. This has isolated the tunnel from all vibration caused by the blower and its motor.

Cylinder Mid-Span Pressure Distributions

The two aluminum cylinders described in the last progress report[10] have been installed in the tunnel. The mid-span static pressure distribution was measured for the cases of a single cylinder on the tunnel centerline, two cylinders with a cylinder separation corresponding to $d/D = 2.2$, and two cylinders with $d/D = 1.5$ ($D = 6.25$ in.). Figures 17, 18 and 19 display these pressure distributions and compare them to the distributions that would exist if the flow were a potential flow around the cylinders mounted in the same test section.

For the case of the single cylinder we obtain the potential flow using the two-dimensional potential flow program (see ref. 10) and calculating the flow past an infinite cascade of single cylinders with the cylinder spacing equal to the width of our test section. For the two double-cylinder cases we calculate the flow past an infinite cascade of groupings of two cylinders where the distance between the two cylinders in any group is given by the value of d/D and the distance between the symmetry lines of two adjacent groups is equal to the test section width. The pressure coefficients are plotted as a function of angle on the cylinder where positive θ is shown in the figures. As expected, for the single cylinder case the measured and potential flow pressure distributions agree quite well in the region of the stagnation point. As one travels tangentially around the cylinder away from the stagnation point, the two distributions differ, due to the effects of increasing boundary layer thickness, separation, etc.

For the case of two cylinders with d/D = 2.2 the stagnation point for both the potential flow and the measured values has moved tangentially inward, with the measured value moving further than the potential value. The flow is most like potential flow on the outer portions of the cylinders and least like potential flow between them. As the cylinders are moved even closer together, d/D = 1.5, the stagnation point moves even further tangentially inward and the deviation from potential flow is of the same sense but everywhere greater in value than for d/D = 2.2. In all cases the pressure distributions are symmetrical about the centerline of the tunnel.

Pressure Reference

A system to supply four known pressures to be used as reference pressures for wind tunnel measurements has been designed and built by a mechanical

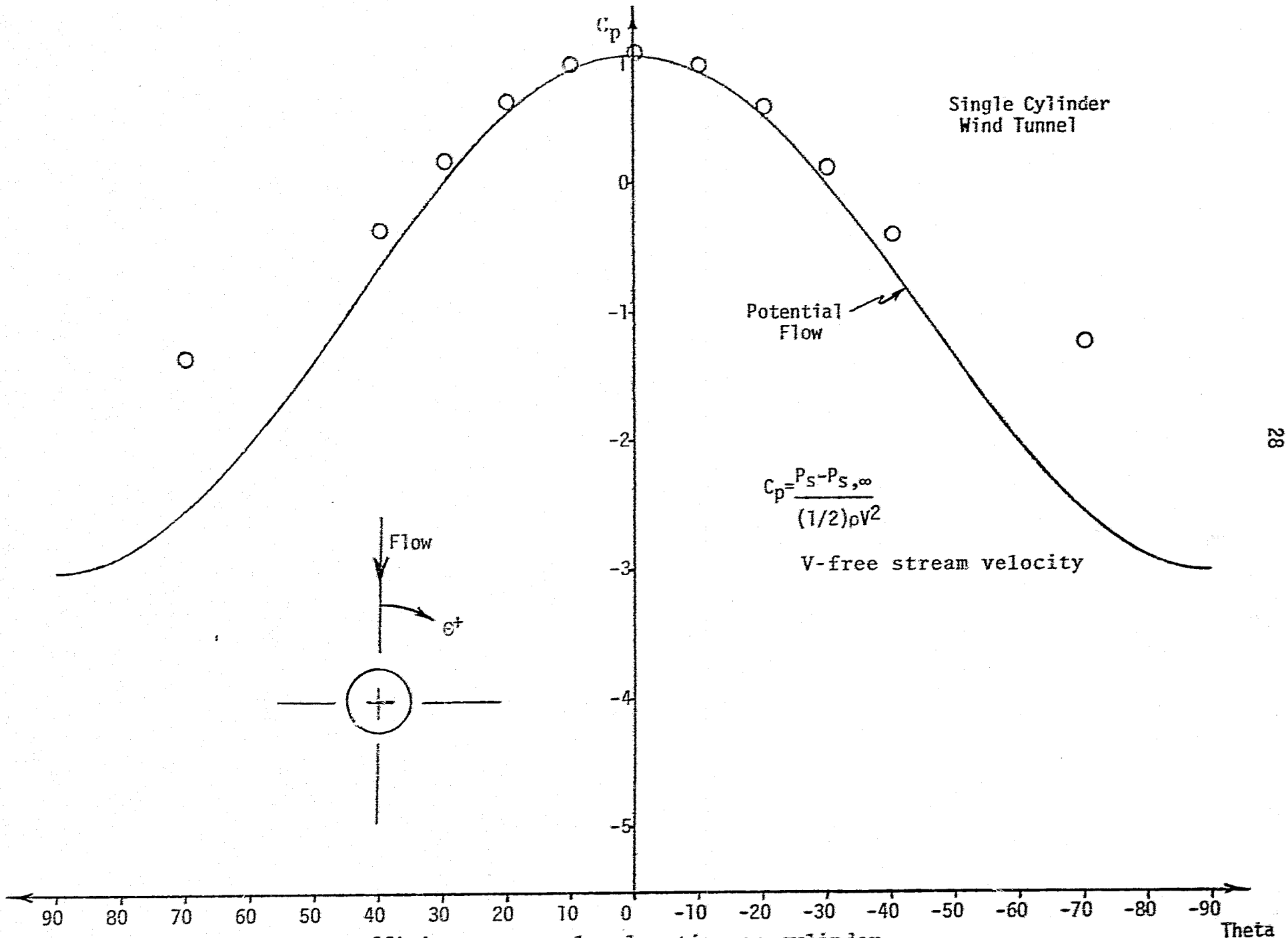

Figure 17 - Pressure coefficient vs angular location on cylinder

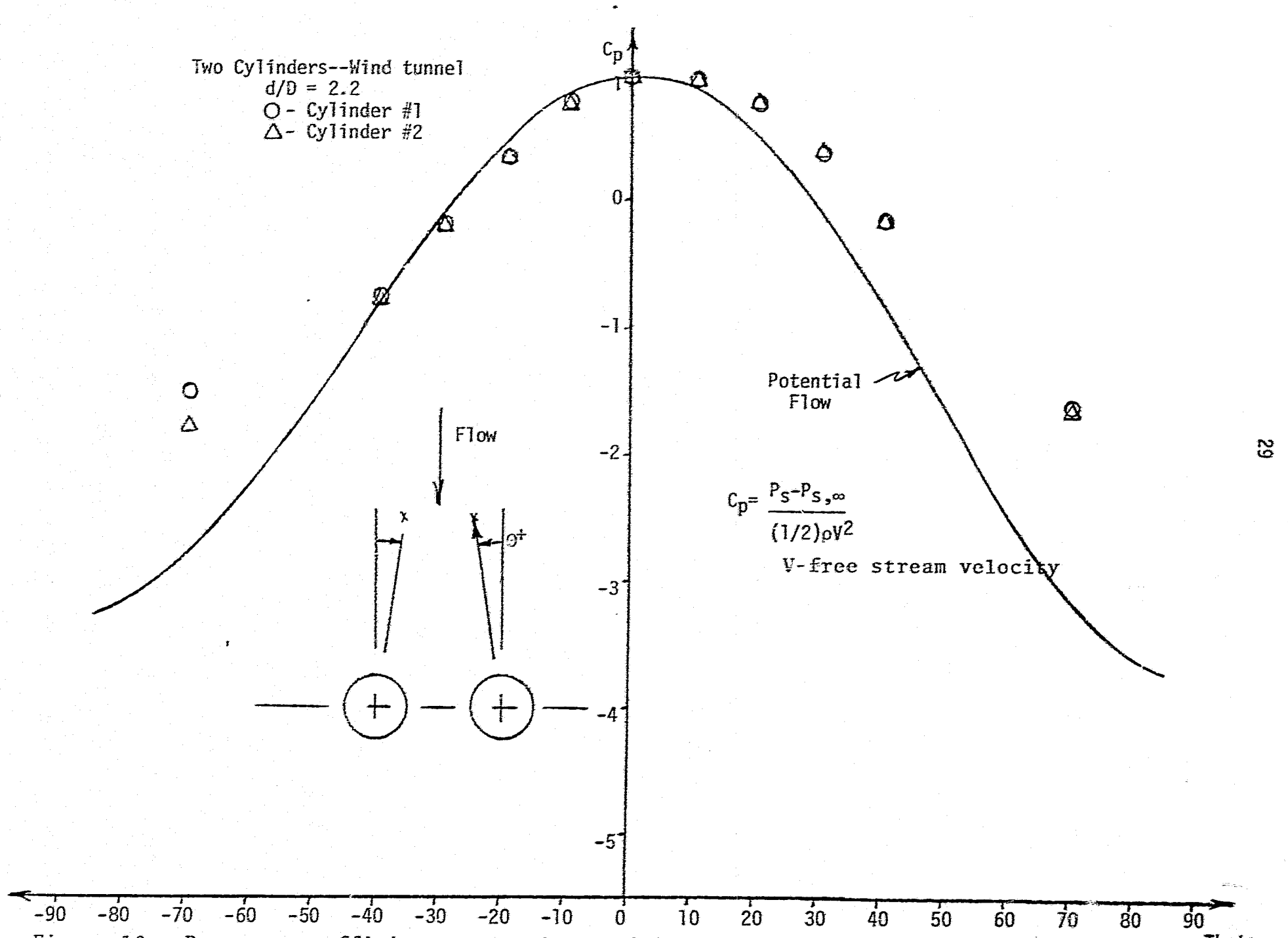

Figure 18 - Pressure coefficient vs angular position on cylinder

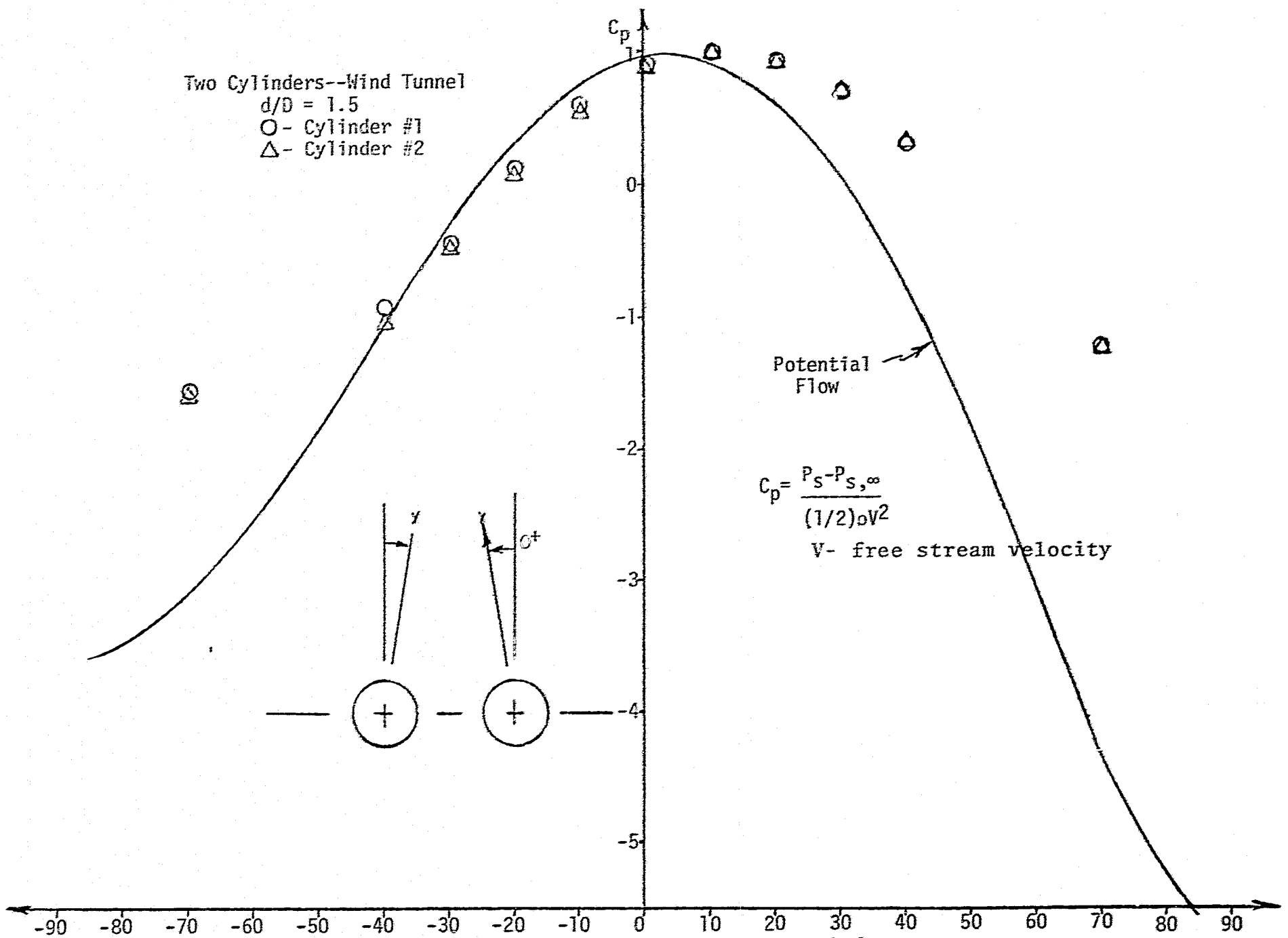

Figure 19 - Pressure coefficient vs angular position on cylinder

engineering senior. Four vertical columns of water of various heights are used to supply reference pressures. A photograph of the four column system is shown in figure 20 and a schematic representation of one column is given in figure 21. The column of water is fixed to the pan of a beam balance (Ohaus Model 1650 cat. #12338-048) and moves up or down with the balance. A thin glass tube with a crook at its lower end extends into the column from above. The tube is fixed in space and therefore does not move with the column. A volume of water (it will become evident that a precise measurement of volume is not necessary) is introduced into the column.

Using a regulated air pressure supply we force the water level in the tube down to a scribed reference line on the horizontal part of the crook. We then adjust the balance to obtain a measurement of the combined column and water mass. Adjusting the balance effects the position of the menicus in the tube therefore this process is repeated until a mass reading can be taken with the meniscus at the reference mark. The supply pressure is then measured using a micromanometer and the mass of the water and column is recorded. Repeating this procedure for a number of different volumes of water yields a calibration relating probe air pressure and mass balance reading so that we can easily supply a known pressure for the wind tunnel pressure transducer scanivalve system. Water levels can be chosen so that the range of pressures to be measured in the wind tunnel is best covered by the reference. One advantage of this system is that tube pressure is fixed by the mass of water in the column and is not affected by room temperature.

Our design goal was a device accurate to within 0.001" of water over the pressure range 0 - 1 psig (27.7" water). The balance is precise to 0.1 grams; therefore, for 0.001" of water to be detected by the balance we must have a minimum column diameter of 2.78" . The diameter of three of the columns

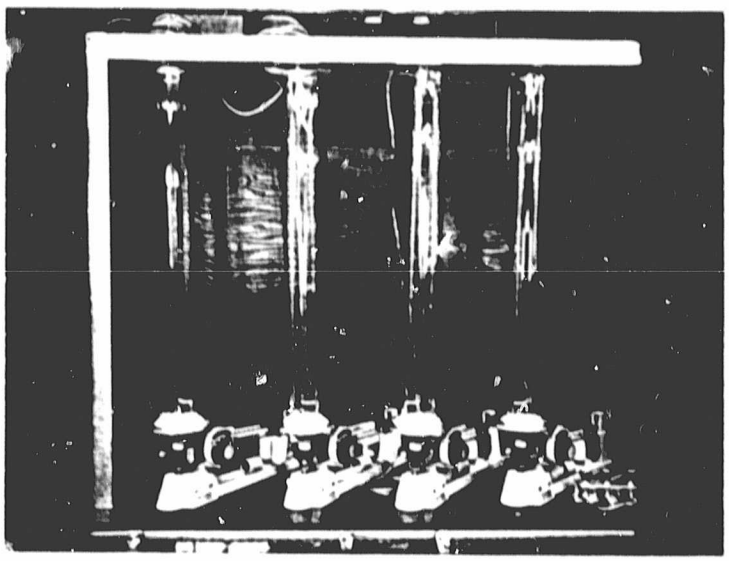

Figure 20 - Photograph of pressure reference system

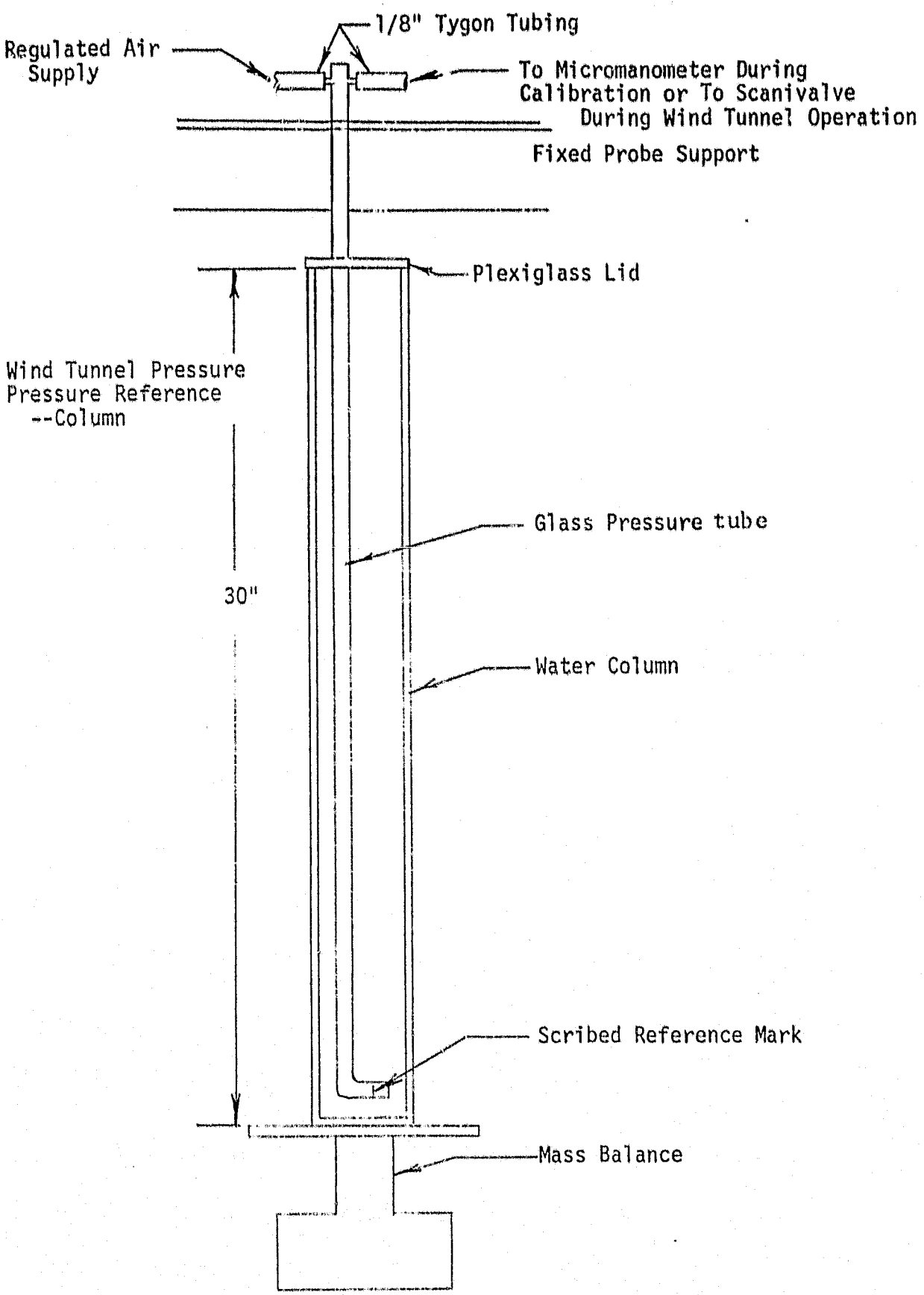

Figure 21 - Wind tunnel pressure reference - Column schematic

used is 3" so that the beam balance precision is adequate. A problem arises in that the balance has a maximum capacity that is reached when a column is filled to 13.8" of water. In order to cover more of the design pressure range we have installed one column with a 2.4" diameter which gives us a range of 21.8" at a resolution of .0013" of water. The Betz micromanometer used for calibration has a 0 - 10" water range and a resolution of 0.001" water.

Overview

The water tunnel tests were completed. Single cylinder data was taken to compare against published data and to identify the important variables. Tests involving two cylinders were run and the results of these tests gave a physical picture of the separation process as the distance between the cylinders is decreased.

The comparison of our single cylinder data to that of Baker[6] has shown some differences in saddle point location trends. As a result of these differences the trends that will be obtained during wind tunnel testing are not obvious. Besides the higher Reynolds numbers obtainable in the wind tunnel we are also capable of varying δ and U independently, therefore uncoupling Re_D and δ/D.

After an intensive search for the causes of observed wind tunnel flow distortion, the variation of the boundary layer thickness on the tunnel endwalls has been eliminated by removal of the inlet honeycomb.

Initial pressure distribution measurements on the cylinders have been made. Work on an important part of the data acquisition system, the pressure reference system, was completed.

Work will continue on the data acquisition system. Meanwhile flow visualization tests in the wind tunnel will be started. On the analysis side of the problem, a student has begun work on the Oswatitsch model.

Acknowledgements

The work reported here has been carried out by Mr. Michael T. Boyle, a graduate student in the Mechanical Engineering Department and by the principal investigator. Mr. James T. Smith, a Mechanical Engineering senior, designed and built the pressure reference system.

Nomenclature

A - flow area

C_{P_T} - total pressure coefficient

d - distance between the centerlines of the two cylinders

D - cylinder diameter

H - shape factor at cylinder position with cylinder absent

k - loss coefficient for screen or perforated plate

$$k = \Delta P/((\tfrac{1}{2})\rho U^2)$$

ℓ - cylinder height

P_T - total pressure, at exit of inlet or at test section

$P_{T,\infty}$ - total pressure, reference probe upstream of cylinders

P_S - static pressure

R - distance from cylinder axis to saddle point

u' - distribution of turbulence within the incoming boundary layer

U - free stream velocity

δ - boundary layer thickness at cylinder position with cylinder absent

δ^* - displacement thickness at cylinder position with cylinder absent

μ - dynamic viscosity

ρ - mass density

$\nu = \mu/\rho$ - kinematic viscosity

References

1. Ram, V. V., "Untersuchungen über die Eckengrenzschicht an einem Kreiszylinder mit Seitenwand," Bericht 63/64, Institut für Strömungsmechanik, Technische Hochschule Braunschweig, 1963.

2. Peake, D. J. and Galway, R. D., "The Three-Dimensional Separation of a Plane Incompressible Laminar Boundary Layer Produced by a Circular Cylinder Mounted Normal to a Flat Plate", High Speed Aerodynamics Section, National Aeronautical Establishment, National Research Council, Ottawa, Canada, 1965.

3. East, L. F. and Hoxey, R. P., "Low-Speed Three-Dimensional Turbulent Boundary Layer Data", Reports and Memoranda No. 3653, Aerodynamics Dept., R.A.E., Bedford, March 1969.

4. Belik, L., "The Secondary Flow About Circular Cylinders Mounted Normal to a Flat Plate", Aeronautical Quarterly, February 1973, pp. 47-54.

5. Baker, C. J., "The Laminar Horseshoe Vortex", J. of Fluid Mechanics, 1979, vol. 95, pp. 347-367.

6. Baker, C. J., "Vortex Flow Around the Bases of Obstacles", A Dissertation submitted to the University of Cambridge, September 1978.

7. Langston, Lee S., "Turbine Endwall Two-Cylinder Program", Semi-Annual Status Report, July 1, 1979 - January 1, 1980.

8. Laws, E. M. and J. L. Livesey, "Flow through Screens", Ann. Rev. Fluid Mech. 1978, 10:247-66.

9. Schubauer, G. B., Spangenberg, W. G. and Klebanoff, P. S., "Aerodynamic Characteristics of Damping Screens", NACA Technical Note 2001, January 1950.

10. Langston, Lee S., "Turbine Endwall Two Cylinder Program", Semi-Annual Status Report, January 1, 1980 - July 1, 1980.